Available online at www.sciencedirect.com
ScienceDirect
Journal of the European Ceramic Society 31 (2011) 1987–1995
www.elsevier.com/locate/jeurceramsoc

Influence of the synthesis conditions on the dielectric properties in the $Bi_{0.5}Na_{0.5}TiO_3$–$KTaO_3$ system

Jakob König *, Matjaž Spreitzer, Danilo Suvorov

Jožef Stefan Institute, Jamova 39, SI-1000 Ljubljana, Slovenia

Received 28 January 2011; received in revised form 29 March 2011; accepted 3 April 2011
Available online 14 May 2011

Abstract

A novel $(1-x)Bi_{0.5}Na_{0.5}TiO_3$–$xKTaO_3$ system was characterized using X-ray powder diffraction, scanning electron microscopy, as well as dielectric and ferroelectric measurements. The results showed the formation of solid solutions across the whole concentration range; however, using a solid-state reaction method it was not possible to obtain single-phase ceramics. The secondary phases formed in the system were alkali-hexatitanate and -tetratantalate. The formation of the solid solutions initially starts with the formation of the $Bi_{0.5}Na_{0.5}TiO_3$- and $KTaO_3$-rich phases, which then react towards the nominal composition at higher temperatures. We observed that the structural and dielectric properties are strongly influenced by the heat-treatment conditions. Typical relaxor properties with a frequency dispersion of the dielectric maximum were obtained only after annealing at a higher temperature, which considerably improved the homogeneity of the perovskite phase. In accordance with the decreasing temperature of the permittivity maximum, ferroelectric measurements showed a changing of the properties from ferroelectric through relaxor to paraelectric with an increasing content of $KTaO_3$.

Keywords: Powders-solid state reaction; Dielectric properties; Perovskites; Microstructure-final; Bi1/2Na1/2TiO3

1. Introduction

The excellent dielectric and piezoelectric properties of the members of the $PbZr_{1-x}Ti_xO_3$ (PZT) and $Pb(Mg_{1/3}Nb_{2/3})O_3$ (PMN) families of ferroelectric and relaxor materials have led to numerous applications in electrical devices, such as actuators, sensors, accelerators, piezoelectric motors, transducers, filters, and resonators.[1] However, despite the exceptional properties of the lead-containing materials, alternative lead-free materials have been under rigorous investigation in the past decade. The most promising lead-free materials come from the alkali-niobium- ($K_{0.5}Na_{0.5}NbO_3$ (KNN)), bismuth-alkali- ($Bi_{0.5}Na_{0.5}TiO_3$ (BNT), $Bi_{0.5}K_{0.5}TiO_3$ (BKT)) and bismuth layer-structured ferroelectrics-based groups.[2] In fact several distinct compositions were found that exhibit specific properties comparable to conventional lead-based materials.[2] For a further improvement of lead-free materials, complex solid solutions with substantial doping will have to be explored, as these provide an increasing number of degrees of freedom for identifying enhanced properties.[3]

BNT,[4,5] with a remanent polarization $P_r = 38\ \mu C/cm^2$, a coercive field $E_c = 73$ kV/cm and high temperature of dielectric maximum $T_m = 320\ ^\circ C$, has been considered to be a good candidate for lead-free piezoelectric ceramics,[2,3] especially when forming a morphotropic phase-boundary (MPB) region in combination with other perovskite materials. The phase sequence of BNT is unique[6] and the nature of the rhombohedral–tetragonal phase transition is not well understood yet. Recently, a new orthorhombic phase was observed in-between the rhombohedral and tetragonal phases by an in situ temperature analysis of the transmission electron diffractions of the structures of BNT.[7] Numerous BNT perovskite-based solid solutions have been investigated for a possible MPB to improve the electromechanical properties and to study the phase transition behaviour of BNT.[8] BNT solid solutions with tetragonal KBT[9,10] and orthorhombic KNN[11,12] have attracted great attention, however, some of the most enhanced electromechanical properties were observed in ternary BNT–BT–KBT[2] and BNT–BT–KNN[13] systems. Among the investigated BNT-based materials, systems with incipient ferroelectrics $SrTiO_3$[14], $CaTiO_3$[15] and $NaTaO_3$[16]

* Corresponding author. Tel.: +386 1 477 3547; fax: +386 1 251 9385.
E-mail address: jakob.konig@ijs.si (J. König).

0955-2219/$ – see front matter © 2011 Elsevier Ltd. All rights reserved.
doi:10.1016/j.jeurceramsoc.2011.04.007

that shift the Curie temperature T_c to lower temperatures have also been reported. $CaTiO_3$ and $NaTaO_3$ additions induce orthorhombic distortion and, additionally, MPB compositions were observed in the BNT-rich part of the systems. In contrast, the occurrence of a strong dispersion of the permittivity with a relaxor-like behaviour within the whole composition range of the solid solutions was observed in the BNT–$SrTiO_3$ system.[14]

Potassium-containing compounds have turned out to be effective additives used to enhance the properties of BNT. Due to the hygroscopic nature of the alkali carbonates and the volatilization-prone Bi, K, and Na components, powder processing and heat treatment are the key factors in controlling the synthesis and microstructure, and, therewith, the repeatability of the electrical properties of such ceramics. Similar processes as observed in the above-mentioned systems are also expected to occur in the $Bi_{0.5}Na_{0.5}TiO_3$–$KTaO_3$ (BNT–KTa) system. The addition of $KTaO_3$ (KTa), which is an incipient ferroelectric, has not been investigated yet and is thus of high scientific interest. The aim of this study was to investigate the solid-state synthesis, the formation of solid solutions and the phase composition of the BNT–KTa system. We focused on the influence of the synthesis conditions on the crystal and phase structure as well as on the dielectric properties of the BNT–KTa system. Additionally, the influence of KTa additions on the ferroelectric properties of BNT was evaluated.

2. Experimental procedure

Ceramic samples with compositions corresponding to the formula $(1-x)Bi_{0.5}Na_{0.5}TiO_3$–$xKTaO_3$ [$(1-x)$BNT–xKTa] were prepared by the solid-state reaction method. Stoichiometric amounts of reagent-grade Na_2CO_3 (Alfa Aesar, Karlsruhe, Germany, 99.997%), K_2CO_3 (Alfa Aesar, 99.997%), Bi_2O_3 (Alfa Aesar, 99.975%), TiO_2 (Alfa Aesar, 99.8%), and Ta_2O_5 (Alfa Aesar, 99.993%) were weighed and mixed thoroughly in an agate mortar under ethanol. Prior to weighing, the Na_2CO_3 and K_2CO_3 powders were dried at 200 °C for 2 h to remove any water content, cooled to room temperature in a silica-gel-filled desiccator and then weighed in air quickly. The mixed powders were dried, uniaxially pressed into pellets under a pressure of 100 MPa and calcined in air at 750 and 850 °C for 10 h with intermediate cooling and grinding. The calcined samples were milled in a planetary mill at 200 rpm for 1 h using 3-mm yttria-stabilized zirconia balls and ethanol media. Then a part of the powder was uniaxially pressed (at 100 MPa) and sintered, while the other part was exposed to high-temperature annealing before the sintering. The annealing was performed at 950 and twice at 1100 °C, each for 10 h. Between the firings the samples were cooled and milled using the same conditions as described above. The high-temperature annealed samples were then cold isostatically pressed (at 750 MPa) and sintered at 1150 °C (1230–1300 °C for sample with 90 mol% of KTa) for 5 h. The preparation procedure for both synthesis paths is shown in Fig. 1. The sintering was performed in a tube furnace in an atmosphere of air with heating and cooling rates of 10 °C/min. Alumina crucibles were used, however, at temperatures above 1000 °C, platinum foil was put under the pellets. The density of the sintered samples was measured using Archimedes' method.

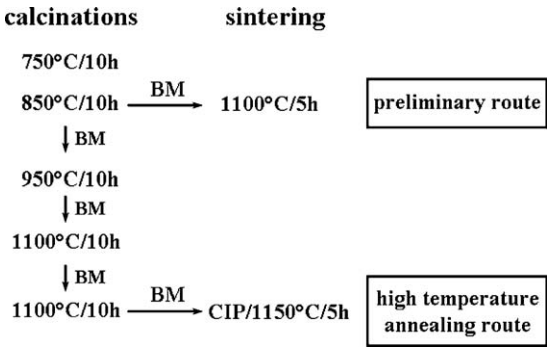

Fig. 1. Preparation of the samples from the $(1-x)$BNT–xKTa system according to the preliminary route and the high-temperature annealing route. (BM: ball milling, and CIP: cold isostatic pressing.)

X-ray powder diffraction (XRD) was used to determine the crystal structure of the samples after each firing. Room-temperature XRD patterns were recorded in the 2θ range 10–70° using a powder diffractometer with Cu K_α radiation (D4 Endeavor, Bruker AXS, Karlsruhe, Germany). The step size and the counting time were 0.04° and 2 s, respectively. In order to enhance the resolution, selected reflections were scanned with a 0.01° step size and 5 s counting time. The XRD patterns were inspected using the EVA software package (Bruker AXS, Karlsruhe, Germany) to identify the phases present. The microstructures of polished sintered samples were observed in a scanning electron microscope (SEM: JEOL JXA 840A, Tokyo, Japan) equipped with an energy-dispersive X-ray spectrometer (EDS). The temperature-dependent dielectric measurements were performed during heating from −180 to 450 °C using an LCR meter (HP 4284A, Hewlett–Packard Co., Palo Alto, CA) at frequencies from 1 kHz to 1 MHz. Silver paste was fired onto the samples at 550 °C for 15 min to serve as the electrode. Polarization–electric field hysteresis loops were measured at room temperature using a Precision LC 10V apparatus (Radiant Technology, Albuquerque, NM) and a 10-kV voltage amplifier (Trek, Medina, NY). The measurements were performed at a frequency of 10 Hz and the amplitude of the applied signal was 90 kV/cm.

3. Results and discussion

3.1. Preliminary route

A preliminary synthesis of the $(1-x)$BNT–xKTa samples with $x = 0.05$, 0.1 and 0.2 was performed as described in Fig. 1. After the first calcination, all the samples exhibited a perovskite main phase as well as a small amount of a secondary phase identified as $Bi_4Ti_3O_{12}$. After a subsequent calcination and sintering, the XRD analyses revealed single-phase samples. However, with the increasing concentration of KTa, the positions of the diffraction peaks were shifted towards lower 2θ values, in accordance with the larger unit cell of the KTa ($V_{pc} = 63.48$ Å^3)[17] compared to the BNT ($V_{pc} = 58.72$ Å^3)[6]. Continuous shifting of the per-

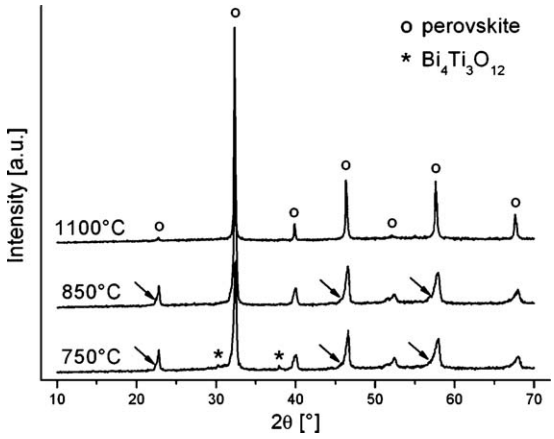

Fig. 2. XRD patterns of the sample with $x = 0.2$ after successive firings at 750 °C, 850 °C and 1100 °C. The arrows indicate broadening of the diffraction peaks.

ovskite peak positions indicates the existence of solid solutions between the BNT and the KTa in the investigated concentration range.

The XRD phase analyses of the sample with $x = 0.2$ after every firing is shown in Fig. 2. After the initial firings the diffraction peaks were very broad and exhibited a tail on the lower 2θ-value side of the diffraction peaks, indicating the inhomogeneous composition of the sample. However, after the firing at 1100 °C the diffraction peaks become narrower and more pronounced. A detailed examination of the diffraction peaks also showed that after the sintering they remained broad for the sample with $x = 0.05$, while the samples with $x = 0.1$ and 0.2 become cubic. The broadening of the peaks for the sample with $x = 0.05$ is discussed later for the sample prepared by the high-temperature annealing route.

The microstructure analysis of the polished samples revealed the presence of small inclusions of a dark secondary phase. Moreover, the sample with $x = 0.2$ (Fig. 3a) also contains some larger grains of a secondary phase. Using EDS, this secondary phase was identified as potassium hexatitanate $K_2Ti_6O_{13}$. However, in some of the secondary-phase grains a part of the potassium was replaced by sodium (up to 10 mol%). The visually estimated volume fraction of the secondary phase in the synthesized samples is below 0.5%. The formation of the $K_2Ti_6O_{13}$ secondary phase indicates similar processes as observed during the synthesis of BKT,[18] where the formation of the potassium polytitanate phase already during calcinations and the volatilization of the potassium and bismuth components during the synthesis were observed. The EDS analysis also revealed that the compositions of the main perovskite phase coincide well with samples' nominal compositions. Nevertheless, the obtained EDS data indicated that the perovskite phase is not completely homogeneous since compositional variations across the main phase are bigger than the analytical error of the method. The inhomogeneity is clearly visible in Fig. 3b, where brighter spots within the main phase are observed. The density of the samples was 94–95% of the theoretical density.

3.2. High-temperature annealing route

In order to eliminate the secondary phase and to improve the homogeneity of the perovskite phase a different synthesis procedure with high-temperature annealing was applied. Additional firings were performed according to the schematic shown in Fig. 1. Samples with x ranging between 0.05 and 0.9 were prepared. After the calcination at 950 °C, the characteristics of the XRD spectra were mainly unchanged when compared to the spectra after the calcination at 850 °C. Obviously, this temperature is not high enough to actuate the homogenization of the perovskite phase. Since the symmetry of the materials in the preliminary study becomes more defined after sintering at 1100 °C, this temperature was selected for additional firings. Two 10-h firings were performed at 1100 °C with intermediate cooling and milling.

The XRD patterns of the sample with $x = 0.2$ prepared by the high-temperature annealing route are shown in Fig. 4. For comparison, a pattern of the sintered sample prepared by the preliminary synthesis is added. Significant changes among the patterns were observed only after high-temperature firings. The intensities of the diffraction peaks at $2\theta \sim 23°$ and 52° decrease with increasing sintering temperature, while the other peaks become sharper and their symmetry characteristics become more evident. These characteristics also indicate a more homogeneous composition of the perovskite phase. All the XRD patterns exhibit a single-phase sample composition.

The XRD patterns of the sintered samples from the $(1-x)$BNT–xKTa system are shown in Fig. 5a. The diffraction peaks are sharp for all the prepared materials, indicating good homogeneity of the perovskite phase after multiple high-temperature firings. With an increasing content of KTa, the peaks are shifted towards lower 2θ values, in accordance with the larger

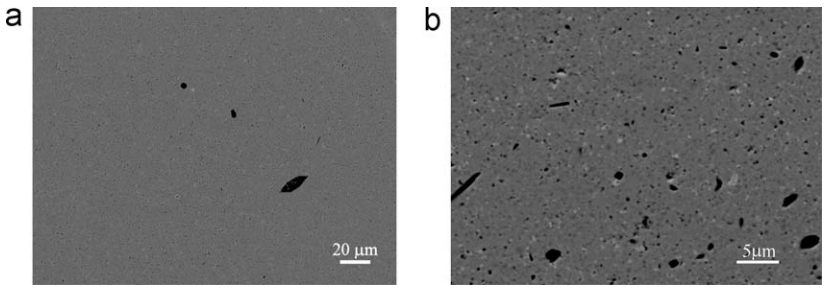

Fig. 3. SEM micrographs of the sintered sample with $x = 0.2$ prepared by the preliminary synthesis: (a) lower magnification, (b) higher magnification with enhanced Z-contrast.

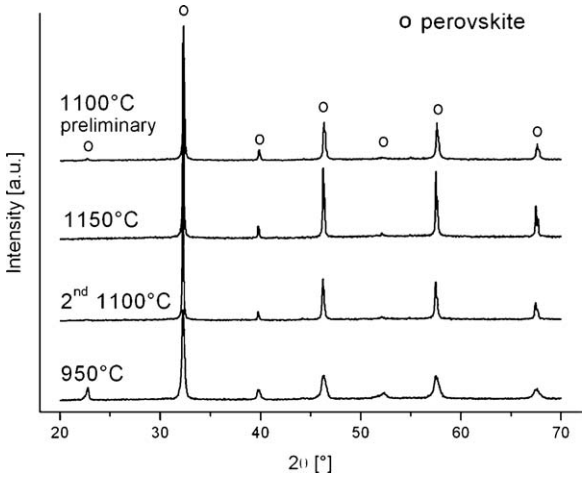

Fig. 4. XRD patterns of the sample with $x = 0.2$ according to the synthesis with high-temperature annealing. For comparison, the XRD pattern of the sintered sample prepared by the preliminary synthesis is added.

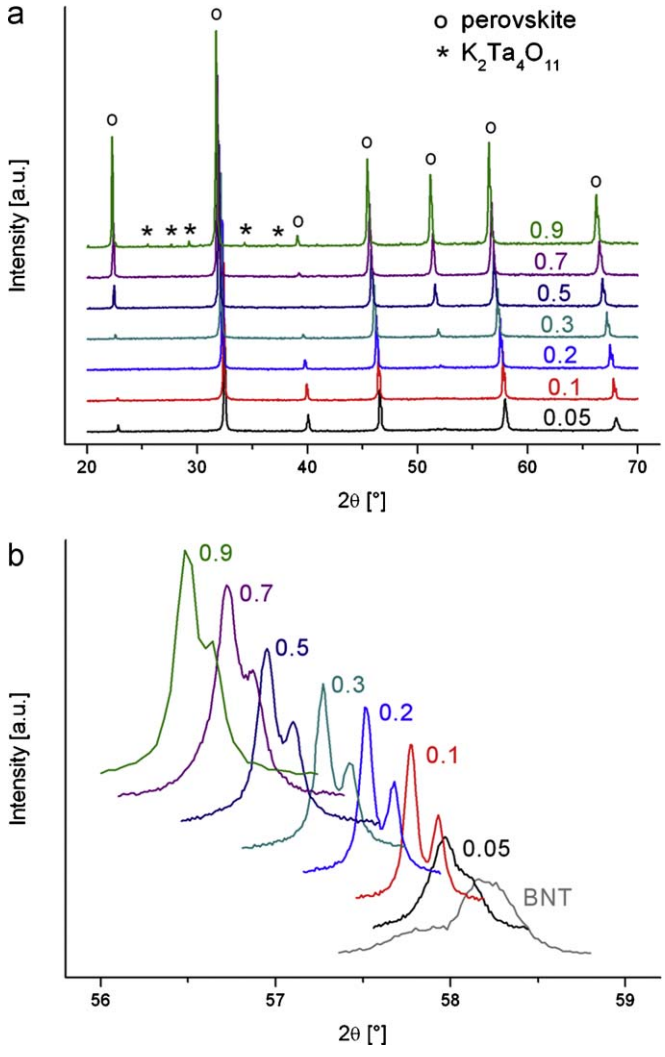

Fig. 5. XRD patterns of the sintered samples from the $(1-x)$BNT–xKTa system prepared according to the synthesis with high-temperature annealing showing (a) 2θ range from 20° to 70° and (b) a detail at $2\theta \sim 57°$. For comparison, data for pure BNT according to the literature[5] are added in (b).

volume of the KTa perovskite cell compared to the BNT. Another feature of the system is a weakening of specific reflections for different compositions; e.g., a weakening of the peak at $2\theta \sim 23°$ for the sample with $x = 0.2$ and the peak at $2\theta \sim 40°$ for the sample with $x = 0.5$. In general, the intensity of the diffracted beam is proportional to the structure factor, which combines the positions of all the atoms in the unit cell together with their scattering powers. Since in BNT–KTa solid solutions many different ions form a unit cell, it is very likely that for a certain composition the atomic scattering factors of different ions cancel each other out for a specific crystal plane and, consequently, the structural factor for this plane is reduced. In such a case the diffraction line that is normally allowed by Bragg's law is weak or even missing. Our experimental data were further proven by the simulation of the diffraction spectra using CaRIne Crystallography[19] software, which showed that for compositions with $x = 0.2$ and 0.5 the intensities of the diffraction lines at $2\theta \sim 23°$ and $2\theta \sim 40°$, respectively, are in fact weakened due to the cancellation of the atomic scattering factors.

The crystal symmetry can be determined from a detailed recording of the diffraction peaks at $2\theta \sim 57°$, which is represented in Fig. 5b. For comparison, the rhombohedral BNT diffraction pattern is added. Samples with x ranging from 0.9 to 0.1 exhibit a cubic symmetry, while the sample with $x = 0.05$ possesses a broad diffraction. For the latter sample, the peak from the $k_{\alpha 2}$ radiation is not so clearly separated from the main peak as for the other samples with cubic symmetry. Compared to the preliminary prepared sample no difference in the XRD pattern for this sample was observed. An additional investigation of the sample with $x = 0.05$ using an X-ray diffractometer equipped with a monochromator confirmed the broad symmetry of the sample with no detectable splitting. Such an observation indicates a smaller rhombohedral distortion with respect to the BNT, which is due to the vicinity of the phase transition. Since we could not determine the rhombohedral and tetragonal or cubic diffraction peaks simultaneously, the existence of a morphotropic phase boundary was ruled out. The macroscopic polar nature of the rhombohedral phase predicted for the sample with $x = 0.05$ is also in accordance with the measured electrical properties for this sample described below. Except in the sample with $x = 0.9$, for which the diffraction peaks of the tetratantalate $K_2Ta_4O_{11}$ phase were observed, no secondary-phase reflections were detected by XRD analyses after the sintering.

Further XRD analyses revealed some additional features of the reaction mechanism in the BNT–KTa system. A comparison of the diffraction patterns for the different compositions shows that after the calcination at 750 °C only the BNT- and KTa-rich phases form (Fig. 6a). In the samples with the KTa concentration below 50 mol% the BNT-rich phase is prevailing and *vice versa*. At higher temperatures these initially formed phases react towards the nominal composition, as seen for the sample with $x = 0.5$ in Fig. 6b. Such behaviour indicates that the perovskite phase is inhomogeneous after the low-temperature firings and since the reaction between the initially formed perovskite phases is slow, high-temperature annealing is needed for the homogenization of the main perovskite phase.

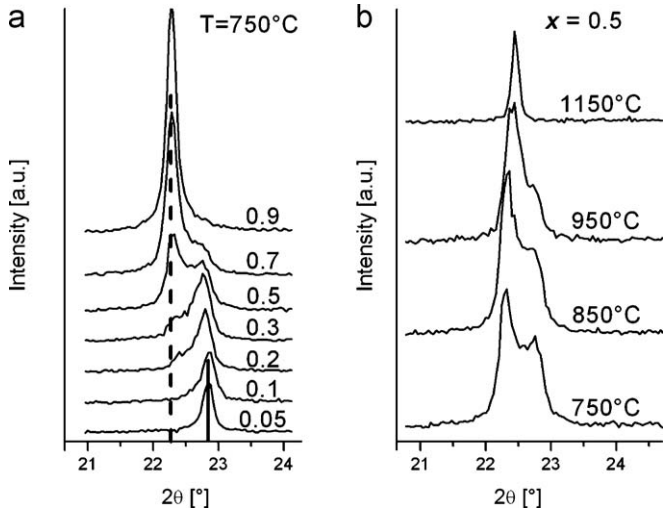

Fig. 6. Evolution of the XRD diffraction lines for (a) the $(1-x)$BNT–xKTa samples with different composition after calcination at 750 °C and (b) the sample with $x = 0.5$ after subsequent firing at different temperatures. In (a) vertical line denotes $Bi_{0.5}Na_{0.5}TiO_3$ diffraction and dotted line denotes $KTaO_3$ diffraction.

Unlike the XRD analyses, the SEM analyses revealed the presence of secondary phases (representative microstructures of the system are shown in Fig. 7). Except for the sample with $x = 0.9$, all the microstructures contained a dark secondary phase, which was identified by means of EDS as $K_2Ti_6O_{13}$, with a part of the potassium replaced by sodium (up to 10 mol%). In the sample with $x = 0.05$, predominantly small inclusions of the secondary phase were present. In addition, large grains of dark secondary phase were also observed; among them some show an anisotropic whisker-like shape. The concentration of large grains increased with the increase of the KTa content up to $x = 0.5$, while in the sample with $x = 0.7$ only small inclusions of dark phase were present again. Compared to the preliminary prepared samples the content of the $K_2Ti_6O_{13}$ secondary phase noticeably increased and was visually estimated to be 1.0–1.5 vol%. In samples with $x = 0.7$ and 0.9, a bright secondary phase was observed. In the sample with $x = 0.7$ only a few large (10–50 μm) rectangular grains of the bright phase were found (Fig. 7d). The sample with $x = 0.9$ showed very poor sinterability and was therefore sintered at 1300 °C; however, the porosity was still high. Moreover, the concentration of the bright secondary phase for that sample strongly increased with the increasing sintering temperature, indicating a rapid decomposition of the main phase. EDS analyses suggested the bright phase to be rich in tantalum (K:Ta ratio ~1:2), which is in accordance with the composition of the $K_2Ta_4O_{11}$ phase, detected by XRD analysis. The EDS analysis of the main perovskite phase also revealed that its composition coincides well with the nominal composition, thus confirming the existence of the solid solutions between the BNT and KTa end members across the whole concentration range. The density of the samples prepared by the high-temperature annealing route was higher (partly because of the additional cold isostatic pressing before sintering) and was above 96% of the theoretical value except for the sample with $x = 0.9$.

According to the results of the XRD and SEM analyses, high-temperature annealing improved the chemical homogeneity of the perovskite phase. A comparison of the microstructures (Figs. 3b and 7c) reveals a smaller contrast and concentration of brighter spots within the perovskite phase in the samples annealed at high temperature. In contrast, the content of the dark phase noticeably increased after several firings at high temperatures. The performed experiments indicate that once the potassium poly-titanate phase is formed, its further reaction towards a compound with the nominal composition is hindered, even by a heat-treatment process, and its concentration increases with additional annealing, which is most probably due to the volatilization from the sample. From the DTA data, the mass loss during the high-temperature annealing for the sample with $x = 0.2$ was estimated to be below 0.5% when

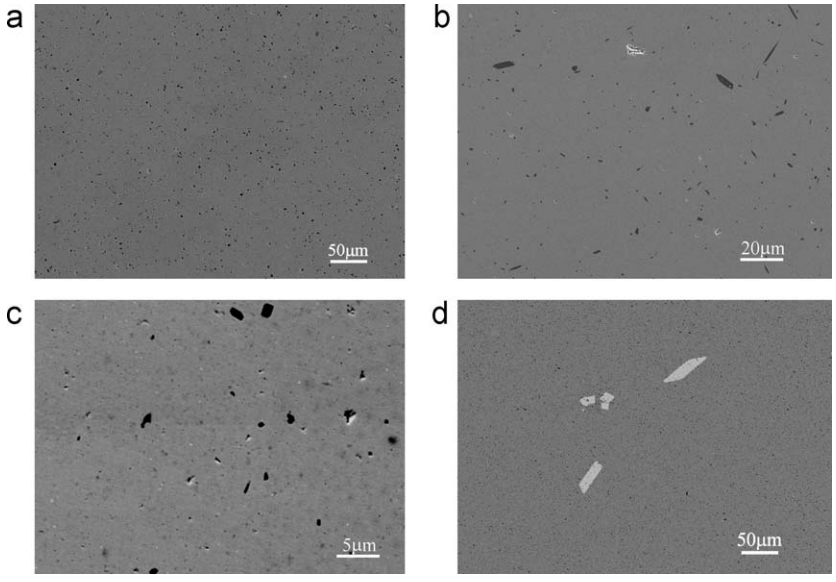

Fig. 7. Selected SEM micrographs of the sintered samples from the $(1-x)$BNT–xKTa system prepared by the synthesis with high-temperature annealing: (a) $x = 0.05$, (b) and (c) $x = 0.2$, (d) $x = 0.7$.

Table 1
Comparison of room-temperature dielectric properties of samples from the $(1-x)$BNT–xKTa system prepared by different procedures.

Compositional fraction x	Preliminary synthesis		Synthesis with high-temperature annealing	
	ε [/]	$\tan\delta$ [/]	ε [/]	$\tan\delta$ [/]
0.05	456	0.055	878	0.056
0.1	780	0.079	1288	0.092
0.2	1156	0.096	1337	0.123

the samples are heat treated in a pellet form. However, the quantification of the losses will be reported in a forthcoming paper on the further optimization of the synthesis. The synthesis behaviour in the BNT–KTa system is similar to the formation mechanism of BKT[18] that involves the same elements as the investigated BNT–KTa system. According to the analysis of the BKT synthesis, the thermal instability of the potassium-containing perovskite phase is responsible for an increased amount of $K_2Ti_6O_{13}$ secondary phase in the high-temperature annealed samples. Nevertheless, according to the EDS results and the shifting of the diffraction lines with the variation of the nominal composition, the solid solutions between BNT and KTa exist across the whole concentration range.

3.3. Dielectric properties

The influence of the synthesis route on the dielectric properties was investigated for samples with $x = 0.05$, 0.1 and 0.2. The dielectric properties of the samples, measured at room temperature and a frequency of 1 MHz, are shown in Table 1. The results show that the samples prepared by the longer route have much higher dielectric constants, almost two times higher in the case of the sample with $x = 0.05$, but also higher dielectric losses. With the improved homogeneity of the perovskite phase in the samples prepared by the high-temperature annealing route, compared to the preliminary prepared samples, the permittivity significantly increases. Such behaviour indicates a change in the properties of the main phase and its higher polarizability. A notable increase in the dielectric losses was observed for the samples with $x = 0.1$ and 0.2, while the increase in the sample with $x = 0.05$ was only minor. Since the increase of the secondary-phase content after high-temperature annealing compared to the preliminary prepared samples in the three compositions is similar, the increase of the losses is most likely also connected with the change in the properties of the main phase.

The temperature dependence of the permittivity for the preliminarily prepared samples is presented in Fig. 8. For comparison the permittivity of the pure BNT prepared according to the literature data[5] is added. With an increasing content of KTa, the permittivity maximum shifts towards lower temperatures, as expected for the addition of an incipient ferroelectric. With the addition of KTa the permittivity maximum also decreases and the hump becomes less evident or it even disappears. However, the decrease of the maximum is not continuous, since the maximum is higher for the sample with $x = 0.2$ compared to the sample with $x = 0.1$. Moreover, the maximum noticeably broadens with an increasing KTa content. The maxima in the dielectric losses coincide with the first half of the permittivity maxima, where the strongest frequency dispersion occurs. Especially in the sample with $x = 0.2$, a smaller hump at higher temperatures can be observed in addition to the main peak. Within the measured frequency range, the dielectric properties show the frequency dispersion of the permittivity, indicating the relaxor nature of the materials. However, the frequency dispersion of the T_m is less evident than that observed in a typical relaxor.[20] A broad permittivity maximum and a rather undefined frequency dispersion of T_m indicate a non-homogeneous composition of the main perovskite phase with polar nano-regions that possess a different relaxation times due to compositional variations.

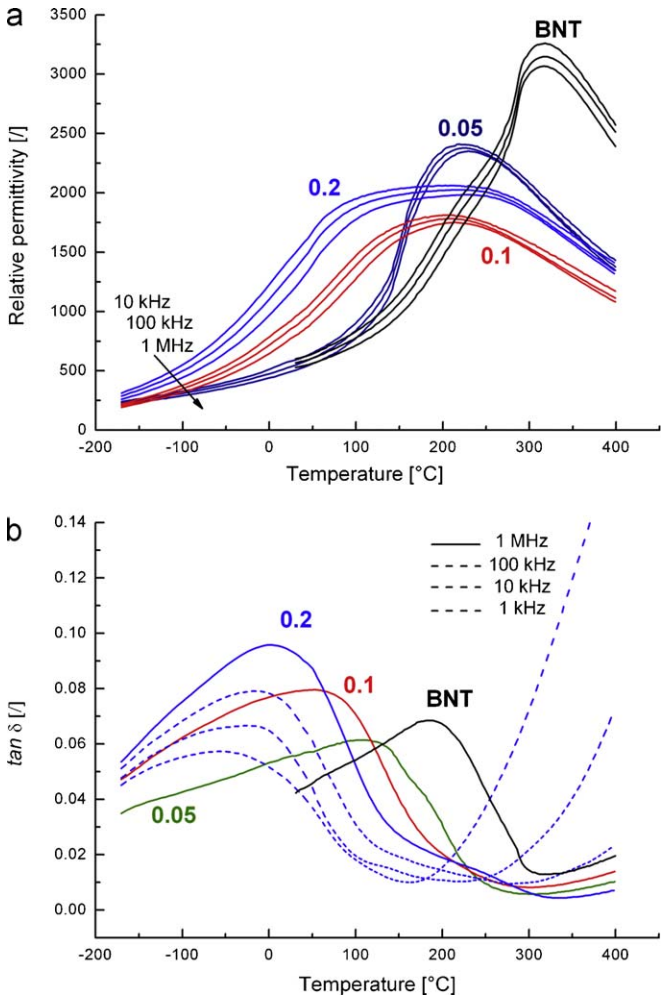

Fig. 8. Temperature dependence of (a) the relative permittivity and (b) the dielectric losses of the preliminary prepared samples from the $(1-x)$BNT–xKTa system. In (b), the dielectric losses at 1 MHz and, additionally, for sample with $x = 0.2$ at 1, 10 and 100 kHz are shown. For comparison, data for pure BNT according to the literature[5] are added.

The dielectric properties of the samples prepared by the high-temperature annealing route are shown in Fig. 9. Some distinctive dielectric characteristics of the BNT–KTa system are:

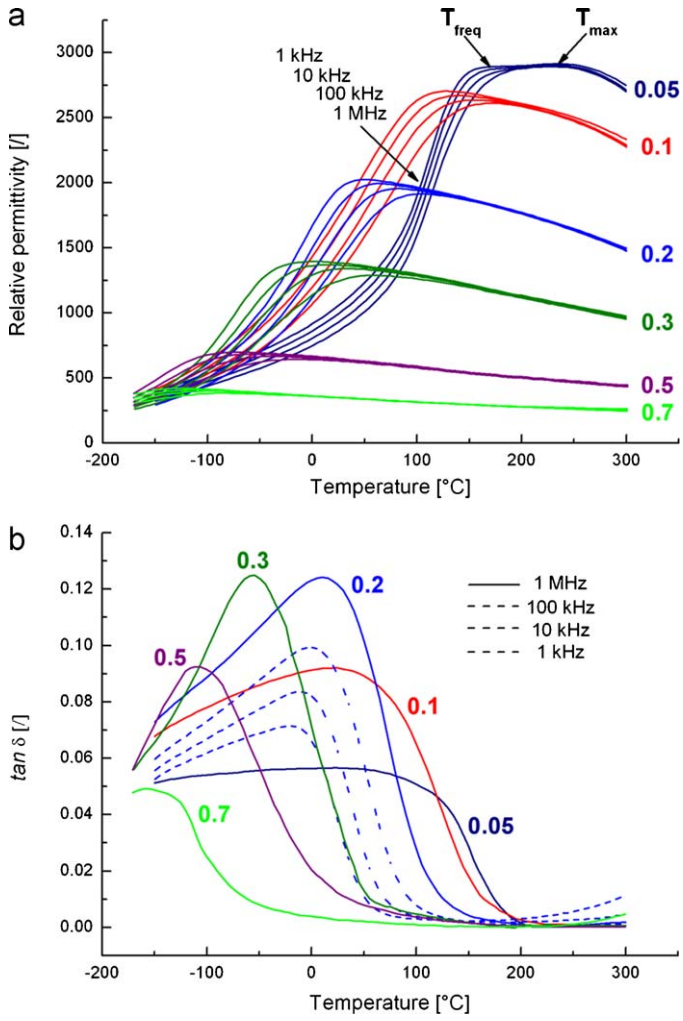

Fig. 9. Temperature dependence of (a) the relative permittivity and (b) the dielectric losses of the high-temperature annealed samples from the $(1-x)$BNT–xKTa system. In (b), the dielectric losses at 1 MHz and, additionally, for sample with $x = 0.2$ at 1, 10 and 100 kHz are shown.

- With an increase of the KTa content, the dielectric maximum is reduced and shifted towards lower temperatures.
- In the sample with $x = 0.05$, the dielectric maximum and the frequency-dispersive anomaly (as observed in pure BNT) are present. Their values of the permittivity are similar, resulting in a broad permittivity maximum.
- In samples with $x \geq 0.1$, only one anomaly remains: the dielectric maximum which shows a distinct frequency dispersion. It is reflected in an anomaly in the dielectric loss curves.
- With an increasing content of KTa, the maximum in the dielectric losses is gradually shifted towards lower temperatures.

A comparison of the dielectric properties of the materials prepared by different routes (Figs. 8 and 9) shows significant differences. In the samples prepared by the high-temperature annealing route the relaxor characteristics of the materials are much more emphasized. Moreover, the permittivity maximum continuously decreases and shifts towards lower temperatures with the increasing content of KTa. The observed changes in the dielectric properties indicate that after the high-temperature annealing polar nano-regions are more uniform due to the improved homogeneity of the main perovskite phase. This improved homogeneity was observed with an XRD analysis that showed sharper diffraction peaks after the multiple firings at high temperatures with respect to the preliminary route. Therefore, typical relaxor properties with a distinct frequency dispersion of the permittivity maximum are observed.

For all the samples a strong temperature and frequency (shown for sample with $x = 0.2$ in Fig. 9b) dependence of the dielectric losses was observed. The temperature interval of the loss tangent maximum coincides with the temperature interval of the maximum frequency dispersion of the dielectric properties. The temperature and the value of the dielectric loss maximum increase as the measurement frequency increases, which are characteristics of a relaxor material.[20] In the temperature range where no frequency dispersion is observed, the dielectric losses are small, below 0.01. The results of the temperature dependence of the dielectric losses showed that a predominant part of the dielectric losses is attributed to the relaxor nature of the perovskite phase. Thereafter, the contribution of the secondary phase(s) to the loss tangent is negligible.

The temperature of the dielectric maximum (at 320 °C in pure BNT) decreases faster than the temperature of the frequency-dispersive anomaly (hump at ~220 °C in pure BNT). In the sample with $x = 0.05$, both anomalies are present, forming a broad dielectric maximum at 160–260 °C (at a frequency of 1 kHz). Such behaviour indicates that the sequence of the phases in this sample remains the same as in pure BNT, and is only shifted towards lower temperatures. On decreasing the temperature, the dielectric losses in sample with $x = 0.05$ start to increase at 190 °C and the loss maximum broadens over a wide temperature range, with a maximum in the room-temperature region. The observed characteristics of the loss maximum, which in the case of the BNT is ascribed to the stabilization of the rhombohedral phase,[5,21] thus indicates a gradual stabilization of the rhombohedral phase. The maximum of the dielectric losses located at 25 °C indicates that the stabilization at room temperature is just completed. However, the newly formed phase has only a small rhombohedral distortion due to the vicinity of the phase transition, which is reflected in the XRD results.

In the sample with $x = 0.1$ only one anomaly is present. The frequency dispersed permittivity maximum is observed closer to room temperature and the maximum of the dielectric losses tightens. This indicates that the phase sequence compared to BNT has changed, and the sample shows typical relaxor behaviour. By connecting the dielectric behaviour with the XRD results, showing the cubic symmetry of the sample, we assume that stable polar regions are dispersed in the cubic non-polar matrix phase. In the samples with $x = 0.2$ and 0.3, the size of these polar regions as well as the correlation among them are further decreased, and the frequency-dispersive maximum is shifted into the room-temperature region. With larger additions of KTa, the dielectric maximum is shifted to below room temperature and a paraelectric character of the samples at room temperature is presumed.

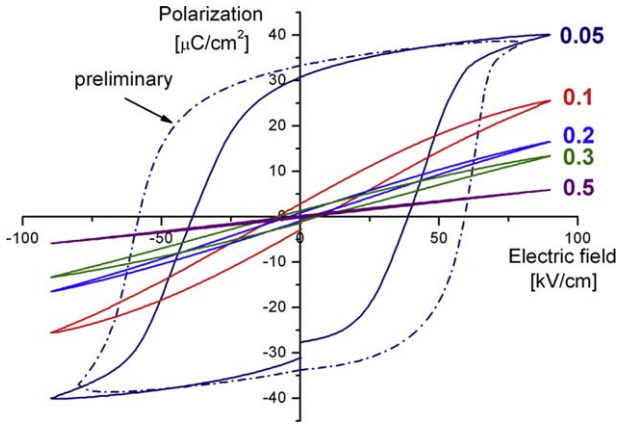

Fig. 10. Polarization–electric field hystereses of samples from the $(1-x)$BNT–xKTa system prepared by the high-temperature annealing route. Broken line shows data for the preliminary prepared sample with $x = 0.05$.

The observed evolution of the dielectric properties with the annealing conditions gives us the possibility to tailor the dielectric properties of such a material for a specific need. When applying only a low-temperature heat treatment, homogenization can be limited. In such a case the material consists of BNT- and KTa-rich regions. The corresponding polar regions, in the compositionally different areas of the material, possess different relaxation times. The broad distribution of the relaxation frequencies results in a broad permittivity maximum with a smaller temperature dependence of the permittivity and a moderate value of the permittivity. In contrast, by applying sufficient temperature and time for the phase homogenization, a composition close to nominal can be achieved. In such a case, the relaxation times of the polar regions are more uniform, resulting in a sharper dielectric maximum with a higher value of the permittivity.

3.4. Ferroelectric properties

The results of the room-temperature hysteresis measurements (Fig. 10) show a decrease in the remanent polarization and the coercive field with an increase of the KTa content. The shape of the hysteresis loops gradually changed from ferroelectric ($x = 0.05$) through relaxor ($0.1 \leq x \leq 0.3$) to paraelectric ($x \geq 0.5$). With an increasing concentration of KTa, the content of the polar (rhombohedral) phase decreases, while the content of the paraelectric (cubic) phase increases. For comparison, a hysteresis of the preliminary prepared sample with $x = 0.05$ is shown in Fig. 10. Both samples with $x = 0.05$ prepared by the different routes exhibit a typical ferroelectric hysteresis; however, the hysteresis of the preliminary prepared sample is more square-shaped with a higher remanent polarization (33 $\mu C/cm^2$) and a higher coercive field (59 kV/cm). These values are closer to the values of pure BNT, since in the preliminary prepared sample the added KTa is incorporated to a lesser extent into the matrix phase, which thus contains a higher content of BNT compared to the high-temperature annealed sample. Similar behaviour was observed in the samples with $x = 0.1$ and 0.2.

In the sample with $x = 0.05$, a typical ferroelectric hysteresis is obtained, indicating that a long-range polar order is maintained. Such results support the interpretation that this sample is rhombohedral, since in the presence of a high-temperature phase the remanent polarization quickly vanishes, as observed for pure BNT above 200 °C.[7] In the sample with $x = 0.1$, a slim hysteresis loop with a small remanent polarization and a relatively high maximum polarization, characteristic for relaxors, is observed. The small value of the remanent polarization is caused by the presence of the cubic phase that separates the polar regions. These are, however, responsible for the high maximum polarization, since the polarization of the regions increases in proportion to the applied electric field. In samples with $x = 0.2$ and 0.3, the content and size of the polar regions decrease, which results in a smaller value of the maximum polarization. However, the shape of the hysteresis retains the relaxor properties, which are supported by the dielectric measurements, as the permittivity maximum is located in the room-temperature region. Since the polar regions are small and their content is low, the XRD analyses showed the cubic symmetry of the samples. In samples with $x = 0.5$ and 0.7, a paraelectric hysteresis loop is observed. Such an observation is in accordance with the results of the dielectric measurements, where a shift of the permittivity maximum to below room temperature was observed for these two samples.

4. Conclusions

The results showed that the formation of the solid solutions between $Bi_{0.5}Na_{0.5}TiO_3$ (BNT) and $KTaO_3$ (KTa) starts with the formation of the BNT- and KTa-rich phases, which then react towards the nominal composition. Better homogeneity of the perovskite phase can be achieved with multiple high-temperature firings. An effective way to follow the homogenization of the main phase is by observing the symmetry of the diffraction lines, which becomes more distinct with increasing homogeneity. However, irrespective of the firing conditions, it was not possible to obtain single-phase ceramics. The secondary phases formed in the system were alkali-hexatitanate and -tetratantalate.

We also showed that the homogeneity of the main perovskite phase has a profound influence on the dielectric properties of the materials, while the influence of the secondary phases was negligible. At room temperature, the permittivity of the high-temperature annealed samples was up to two times the permittivity of the samples heat treated only at lower temperatures. The relaxor dielectric properties for samples with an inhomogeneous main phase were less evident than for the high-temperature annealed samples with a substantially higher homogeneity of the main perovskite phase. In the latter case, the dielectric maximum with a clear frequency dispersion was continuously shifted towards lower temperatures with an increasing KTa content and, additionally, its maximum value continuously decreased. The observed evolution of the dielectric properties gives us the possibility to tailor the dielectric properties of such a material with the proper choice of the firing conditions. The polarization–electric field hysteresis properties of the samples

gradually changed from ferroelectric through relaxor to paraelectric with an increasing KTa content.

Acknowledgements

The research was financially supported by the Ministry of Higher Education, Science and Technology of the Republic of Slovenia, under Grant No. 3311-04-831066 and by the EPCOS OHG, a group company of the TDK-EPC Corporation.

References

1. Uchino K. *Ferroelectric devices*. Marcel Dekker: New York; 2000.
2. Takenaka T, Nagata H, Hiruma Y. Current developments and prospective of lead-free piezoelectric ceramics. *Japanese Journal of Applied Physics* 2008;**47**:3787–801.
3. Aksel E, Jones JL. Advances in lead-free piezoelectric materials for sensors and actuators. *Sensors* 2010;**10**:1935–54.
4. Smolenskii GA, Isupov VA, Agranivyskaya AI, Krainik NN. New ferroelectrics of complex composition. IV. *Soviet Physics: Solid State* 1961;**2**:2651–4.
5. Spreitzer M, Valant M, Suvorov D. Sodium deficiency in $Na_{0.5}Bi_{0.5}TiO_3$. *Journal of Materials Chemistry* 2007;**17**:1–9.
6. Jones GO, Thomas PA. Investigation of the structure and phase transitions in the novel A-site substituted distorted perovskite compound $Na_{0.5}Bi_{0.5}TiO_3$. *Acta Crystallografica* 2002;**B58**:168–78.
7. Dorcet V, Trolliard G, Boullay P. The structural origin of the antiferroelectric properties and relaxor behavior of $Na_{0.5}Bi_{0.5}TiO_3$. *Journal of Magnetism and Magnetic Materials* 2009;**321**:1758–61.
8. Rödel J, Jo W, Seifert KTP, Anton E-M, Grancow T, Damjanovic D. Perspective on the development of lead-free piezoceramics. *Journal of the American Ceramic Society* 2009;**92**:1153–77.
9. Sasaki A, Chiba T, Mamiya Y, Otsuki E. Dielectric and piezoelectric properties of $(Bi_{0.5}Na_{0.5})TiO_3$–$(Bi_{0.5}K_{0.5})TiO_3$ systems. *Japanese Journal of Applied Physics* 1999;**38**:5564–7.
10. Otoničar M, Škapin SD, Spreitzer M, Suvorov D. Compositional range and electrical properties of the morphotropic phase boundary in the $Na_{0.5}Bi_{0.5}TiO_3$-$K_{0.5}Bi_{0.5}TiO_3$ system. *Journal of the European Ceramic Society* 2010;**30**:971–9.
11. Kounga AB, Zhang ST, Jo W, Granzow T, Rodel J. Morphotropic phase boundary in $(1-x)Bi_{0.5}Na_{0.5}TiO_{3-x}K_{0.5}Na_{0.5}NbO_3$ lead-free piezoceramics. *Applied Physics Letters* 2008;**92**:222902.
12. Zuo RZ, Fang XS, Ye C. Phase structures and electrical properties of new lead-free $(Na_{0.5}K_{0.5})NbO_3$–$(Bi_{0.5}Na_{0.5})TiO_3$ ceramics. *Applied Physics Letters* 2007;**90**:092904.
13. Zhang ST, Kounga AB, Aulbach E, Ehrenberg H, Rödel J. Giant strain in lead-free piezoceramics $Bi_{0.5}Na_{0.5}TiO_3$–$BaTiO_{3-x}K_{0.5}Na_{0.5}NbO_3$ system. *Applied Physics Letters* 2007;**91**:112906.
14. Krauss W, Schütz D, Mautner FA, Feteira A, Reichmann K. Piezoelectric properties and phase transition temperatures of the solid solution of $(1-x)(Bi_{0.5}Na_{0.5})TiO_{3-x}SrTiO_3$. *Journal of the European Ceramic Society* 2010;**30**:1827–32.
15. Ranjan R, Garg R, Kothai V, Agrawal A, Senyshyn A, Boysen H. Phases in the $(1-x)Na_{0.5}Bi_{0.5}TiO_3$–$(x)CaTiO_3$ system. *Journal of Physics: Condensed Matter* 2010;**22**:075901.
16. König J, Jančar B, Suvorov D. New $Na_{0.5}Bi_{0.5}TiO_3$–$NaTaO_3$-based perovskite ceramics. *Journal of the American Ceramic Society* 2007;**90**:3621–7.
17. Zhurova EA, Ivanov Y, Zavodnik V, Tsirelson V. Electron density and atomic displacements in $KTaO_3$. *Acta Crystallografica* 2000;**B56**:594–600.
18. König J, Spreitzer M, Jančar B, Suvorov D, Samardžija Z, Popović A. The thermal decomposition of $K_{0.5}Bi_{0.5}TiO_3$ ceramics. *Journal of the European Ceramic Society* 2009;**29**:1695–701.
19. Boudias C, Monceau D. *CaRIne Crystallography Software*, http://pros.orange.fr/carine.crystallography (1989–2005).
20. Bokov AA, Ye Z-G. Recent progress in relaxor ferroelectrics with perovskite structure. *Journal of Materials Science* 2006;**41**:31–52.
21. Suchanicz J. Investigations of the phase transitions in $Na_{0.5}Bi_{0.5}TiO_3$. *Ferroelectrics* 1995;**172**:455–8.